



# Influence of air-cooled heat dissipation on the thermal characteristics and thermal management of battery packs for electromechanical equipment under plateau environment

Yunfei Yan<sup>1</sup> · Yonghong Wu<sup>1</sup> · Rongtian Wang<sup>1</sup> · Ziqiang He<sup>2</sup> · Jinhua Wu<sup>1</sup> · Jingxiang You<sup>1</sup> · Zongguo Xue<sup>1</sup>

Received: 8 October 2023 / Accepted: 19 May 2024 / Published online: 18 June 2024  
© Akadémiai Kiadó, Budapest, Hungary 2024

## Abstract

As the plateau environment is characterized by low air pressure and low density, it greatly limits the heat dissipation performance of high-power electromechanical equipment. Especially for new military combat equipment in China, such as hybrid armored vehicles, effective heat dissipation of power batteries is essential for their operational viability in intricate plateau terrains. This paper focuses on the thermal management and heat dissipation attributes of a lithium-ion battery assembly within a military hybrid armored vehicle stationed at an altitude of 4000 m. Firstly, a comprehensive three-dimensional thermal model was constructed for the battery unit to establish an air-cooled dissipation framework. Secondly, the effect of structural parameters of the battery pack, specifically inlet and outlet sizes, quantity, and layouts, on heat dissipation was investigated. The results indicate that larger air inlet and outlet sizes contribute to better battery pack heat dissipation. And using two air inlets and outlets not only leads to lower maximum temperatures but also enhances overall temperature uniformity and cell module temperature consistency. Additionally, the forced convective heat transfer was analyzed by investigating the influence of inlet velocity. It was observed that forced air-cooled is suitable for battery packs with discharge rates below 1.6 C. Strategic optimization of battery pack structural parameters and the adoption of the carrier air-cooled approach can notably enhance battery cooling efficacy in plateau environments. These insights serve as a blueprint for refining battery pack designs to bolster heat dissipation performance, ultimately bolstering stability and reliability in plateau environments.

**Keywords** Hybrid armored vehicle · Plateau environment · Lithium-ion battery · Thermal management

## Introduction

The field of electromechanical equipment spans a wide array of applications encompassing various aspects of production and daily life [1–3]. It finds extensive applications in mechanical, electrical, abrasive design and manufacturing, automotive industries, as well as testing [4–9]. With the rapid growth of the economy, an increasing number of enterprises and industries are recognizing the significance of

incorporating mechanical and electrical equipment into their production and operational processes [10–12].

Plateau environment generally refers to elevated regions above 1500 m above sea level. These areas are characterized by low atmospheric pressure, thin air, and substantial temperature fluctuations between day and night, significantly differing from those at lower altitudes [13]. The most apparent feature is the reduction in atmospheric pressure. The dissipation of heat in electromechanical equipment primarily relies on air convection [14]. However, the decrease in atmospheric pressure leads to a decline in air density and air flow per unit volume, thereby weakening the convective heat transfer effect. This poses considerable challenges to the heat dissipation performance of electromechanical equipment, ultimately affecting its normal operation and functionality. Consequently, research into methods for enhancing the heat dissipation of mechanical and electrical equipment in plateau environments becomes an urgent problem.

✉ Yunfei Yan  
yunfeiyan@cqu.edu.cn

<sup>1</sup> Key Laboratory of Low-Grade Energy Utilization Technologies and Systems, Chongqing University, Ministry of Education, Chongqing 400030, China

<sup>2</sup> Key Laboratory of Electromechanical Equipment Security in Western Complex Environment for State Market Regulation, Chongqing 401121, China

Numerous scholars have conducted research on the heat dissipation of electromechanical equipment in high-altitude regions. Steinberg et al. [15] analyzed the performance equation of printed circuit boards (PCBs) under uniform heat transfer, considering the effect of air density changes on the dissipation of heat from electromechanical equipment in elevated regions. Their findings emphasize the importance of accounting for air density fluctuations to prevent excessive pressure drops and ensure sufficient airflow for cooling. Belady et al. [16] examined the influence of altitude on flow characteristics and heat transfer in equipment, highlighting the role of altitude alterations on fan airflow through Fan Laws. Hall et al. [17] focused on exploring the effect of altitude on electronic device heat dissipation, measuring and comparing the heat source temperature of two identical PCB boards in two cities with different altitudes through experimental methods. Xun et al. [18] compared measurement data obtained at high altitudes with those gathered on the ground, utilizing dimensionless correlation methods to assess temperature rise changes in high-power electromechanical equipment. Wong et al. [19] investigated the effect of altitude and changes in wind speed on electronic devices heat dissipation by constructing a low-pressure wind tunnel to simulate environmental conditions in plateau regions. Esayed et al. [20] evaluated the heat dissipation characteristics of an air-cooled forced convection system within an aircraft wing compartment at altitudes ranging from 0 to 12,000 m. Their study also examined the thermal resistance of the radiator under different fin configurations. Jordi et al. [21] designed a high-temperature proton exchange membrane fuel cell, demonstrating the effectiveness of cooling system in maintaining the battery temperature of light UAVs below 160 °C at altitudes ranging from 0 to 10,000 m.

The heat dissipation issue in hybrid armored vehicles arises mainly from the use of lithium-iron phosphate batteries. These batteries produce substantial heat during operation [22–24], and the battery life would be affected if the heat could not be discharged in time. There is limited space in military armored vehicles for special reasons, such as requiring the storage of a substantial amount of military equipment. Due to the low cost and lightweight characteristics of air cooling, researchers have extensively explored air-cooled heat dissipation solutions for lithium batteries installed in hybrid armored vehicles. Xu et al. [25] conducted a simulated air-cooled experiment within the battery compartment, analyzing heat dissipation under operating conditions of 1 C and a wind speed of  $4\text{ms}^{-1}$ . Their findings demonstrate a reduction of 4.57 °C, 4.3 °C, and 3.65 °C, respectively, in average temperature, maximum temperature, and temperature differential within the battery compartment after incorporating a guide plate. By introducing a baffle, the air-cooled effects were enhanced, resulting in improved temperature uniformity between modules and enabling the modules to

operate at more suitable ambient temperatures. Xie et al. [26] investigated the influence of inlet and outlet angles, and channel width between battery units on lithium-ion battery pack heat dissipation. Through single-factor analysis and orthogonal testing, three structural parameters were optimized. The results reveal that optimum cooling performance was achieved with an inlet angle of 2.5°, outlet angle of 2.5°, and equal channel width. Additionally, Husam et al. [27] examined the heat dissipation characteristics of air-cooled with varying spacing between batteries, specifically from 2 to 6 mm. Their findings indicate that greater spacing leads to higher average Nussel numbers, thus enhancing heat dissipation performance.

In conclusion, air cooling presents significant advantages for thermal management of mechanical and electrical equipment in plateau and high-altitude environments due to its low cost and portability. This paper focuses on the lithium-iron phosphate power battery pack employed in military hybrid armored vehicles, investigating its heat dissipation characteristics and thermal management in a high-altitude plateau at 4000 m. Besides, this paper mainly evaluates the performance of lithium-iron phosphate power battery under air-cooled heat dissipation conditions.

## Numerical method

### Physical model

Firstly, a three-dimensional geometric model of the lithium-ion battery was established. Due to the intricate internal structure of the lithium-ion battery, comprising diverse materials arranged in multiple layers, direct modeling would prove excessively time-consuming. Therefore, a simplified model of the battery unit was devised, encompassing the entirety of the interior structure, while disregarding variations in heat production within the battery. The lithium-ion battery model established in this paper is shown in Fig. 1. For an individual cell (a), the dimensions are as follows: length—130 mm, width—36 mm, height—185 mm, with a pole post height of 10 mm. A single battery module encompasses nine lithium-ion battery units (b). Utilizing these lithium-ion units as a foundation, an air-cooled heat dissipation model (c) was formulated for the lithium-ion battery pack. In this investigation, the dimensions of the battery pack in the air-cooled thermal model (c) measure 820 mm in length, 424 mm in width, and 265 mm in height. The original air inlet and outlet ports for airflow are positioned on the transverse walls on either side of the battery pack, employing a singular inlet and outlet airflow configuration. Circular inlet and outlet shapes were regulated, with an initial diameter of 120 mm. The layout dimensions of the battery pack are shown

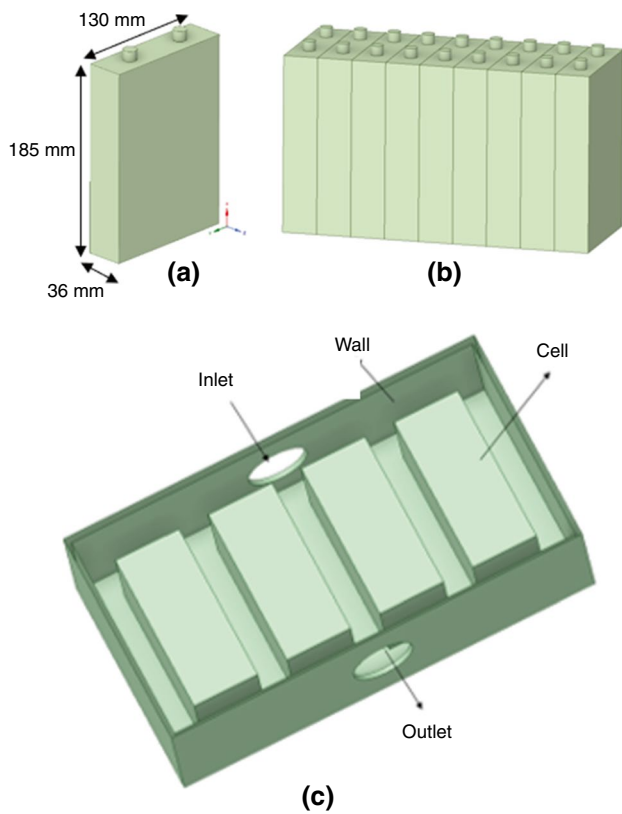


**Fig. 1** Geometric structure of the battery module. **a** Single lithium-ion battery; **b** lithium-ion battery pack; **c** 3D diagram of the BTMS

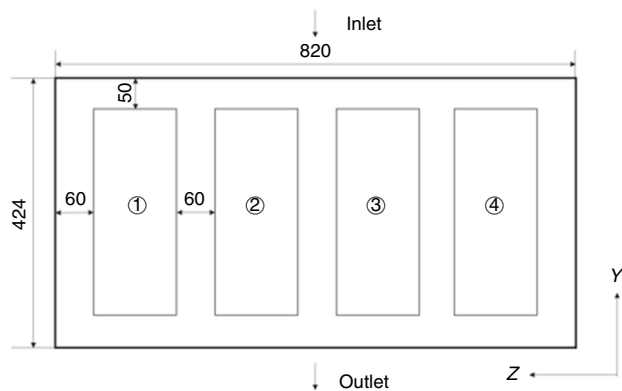


**Fig. 2** 2D diagram of the BTMS

**Table 1** Properties of the air and battery cell

Property	Air (height at 4000 m)	Value
Density/kgm <sup>-3</sup>	0.819	1862.8
Specific heat/Jkg <sup>-1</sup> K <sup>-1</sup>	1005	1150
Dynamic viscosity/kgm <sup>-1</sup> s <sup>-1</sup>	2.187 × 10 <sup>-5</sup>	–
Thermal conductivity/Wm <sup>-1</sup> K <sup>-1</sup>	2.304	λ <sub>y</sub> :0.9;λ <sub>x</sub> λ <sub>z</sub> :15.3
Initial temperature/K	288.15	288.15
Heat generated of each battery at 1 C/Wm <sup>-3</sup>	–	8650

in Fig. 2, while the properties of both the air and battery cell are detailed in Table 1.

**Numerical description**

This study employed the CFD method to compute the temperature and flow patterns of the BTMS. The assessment of cooling performance for each BTMS was based on the maximum battery temperature ( $T_{max}$ ) and the greatest temperature differential ( $\Delta T_{max}$ ) across four batteries. Here, battery temperature denotes the mean temperature of individual battery cell. Battery thermal management primarily involves convective heat transfer, with the governing equations outlined as follows [28, 29].

Continuity equation:

$$\nabla \cdot \vec{u} = 0 \tag{1}$$

$\vec{u}$  indicates the flow velocity vector.

Momentum conservation equation:

$$\rho \frac{d\vec{u}}{dt} = -\nabla p + \mu \nabla^2 \vec{u} \tag{2}$$

$\rho$  and  $\mu$  represent fluid density and dynamic viscosity, respectively, while  $p$  denotes pressure.

Energy conservation equation:

$$\rho C_p \frac{\partial T}{\partial t} + \nabla \cdot (\rho C_p \vec{u} T) = \nabla \cdot (k \nabla T) \tag{3}$$

$C_p$  and  $k$  demonstrate the specific heat and thermal conductivity of the fluid, while  $T$  denotes the fluid temperature.

In this investigation, the value of  $y^+$  was small, indicating that the Reynolds number, based on the inlet velocity of the BTMS, exceeded 3000, reaching 10,566. Consequently, the flow regime within the BTMS was classified as turbulent. For the calculation of turbulent flow, the standard k-ε model with an improved wall treatment was utilized. The governing equations for turbulent flow are delineated as follows [30, 31].

Turbulent kinetic energy equation:

$$\rho \frac{\partial k}{\partial t} + \rho u_j \frac{\partial k}{\partial x_j} = \left[ \eta + \frac{\eta_t}{\sigma_k} \frac{\partial k}{\partial x_j} \right] + \eta_i \frac{\partial u_i}{\partial x_j} \left( \frac{\partial u_i}{\partial x_j} + \frac{\partial u_j}{\partial x_i} \right) - \rho \epsilon \quad (4)$$

Turbulent kinetic energy dissipation equation:

$$\rho \frac{\partial \epsilon}{\partial t} + \rho u_k \frac{\partial \epsilon}{\partial x_k} = \left[ \eta + \frac{\eta_t}{\sigma_\epsilon} \frac{\partial \epsilon}{\partial x_k} \right] + \frac{c_1 \epsilon}{k} \eta_i \frac{\partial u_i}{\partial x_j} \left( \frac{\partial u_i}{\partial x_j} + \frac{\partial u_j}{\partial x_i} \right) - c_2 \rho \frac{\epsilon^2}{k} \quad (5)$$

in this equation,  $\eta_t$  is turbulence viscosity coefficient,  $c_1$ ,  $c_2$  and  $c_u$  are three empirical coefficients, and  $\sigma_k$ ,  $\sigma_\epsilon$ , and  $\sigma_T$  are three constants, the general values are shown in Table 2.

Additionally, the numerical simulations incorporated the following assumptions. (1) The cooling air was assumed to be incompressible. (2) Heat dissipation within the battery pack was solely attributed to the battery discharge process, treating the heat output of battery module as constant. (3) Radiation heat transfer emitted by the battery was disregarded [32].

Moreover, this study established the battery pack wall boundary and the surrounding environment as sites of convective heat transfer. The convective heat transfer coefficient was determined to be  $5 \text{ W m}^{-2} \text{ K}^{-1}$ , while the ambient temperature was defined as the maximum daily average temperature ( $T_{\text{ambient}}$ ), set at  $15 \text{ }^\circ\text{C}$  for the 4000 m plateau [33]. The inlet boundary was designated as a velocity inlet boundary, with the natural convection wind speed set at  $5 \text{ ms}^{-1}$  in plateau environment, and the air temperature at the inlet matched the ambient temperature.

Utilizing ANSYS FLUENT, the resolution of flow and temperature fields was executed, encompassing fluid–solid coupling for heat transfer, thus demanding the utilization of the simple algorithm for velocity–pressure coupling. To harmonize the calculation time and accuracy, the continuity equation was set to achieve a root mean square error of less than  $10^{-4}$ . Similarly, for the energy equation, velocity

components, as well as  $k$  and epsilon, the root mean square error was set to under  $10^{-6}$ . The hybrid initialization method was utilized for simulation initialization, and the calculations were executed until convergence was attained.

## Grid dependence analysis

Fluent meshing was employed to construct the three-dimensional geometric model mesh for air-cooled heat dissipation. To guarantee mesh quality, convergence, and accuracy, a polyhedral mesh was utilized. The minimum unit length was configured at 0.8 mm, while the maximum unit was capped at 2.8 mm. The mesh diagram of the model is depicted in Fig. 3.

Grid independence verification was conducted to ensure that the simulation results remained unaffected by the number of grids and to conserve computing resources. The grid independence results are shown in Fig. 4. Under the condition of 1 C discharge multiplier, the number of grids was set to 68,563, 194,553, 280,498, and 760,765, respectively. Upon increasing the grid count from 280,498 to 760,765, the maximum temperature of the battery pack exhibited a slight change, approximately 0.75%, falling within an acceptable margin of error attributable to grid variations. Consequently, a grid count of 280,498 was deemed sufficient for calculating all BTMSs in this study.

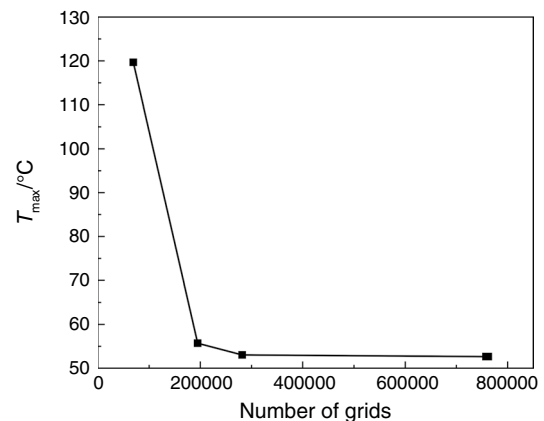
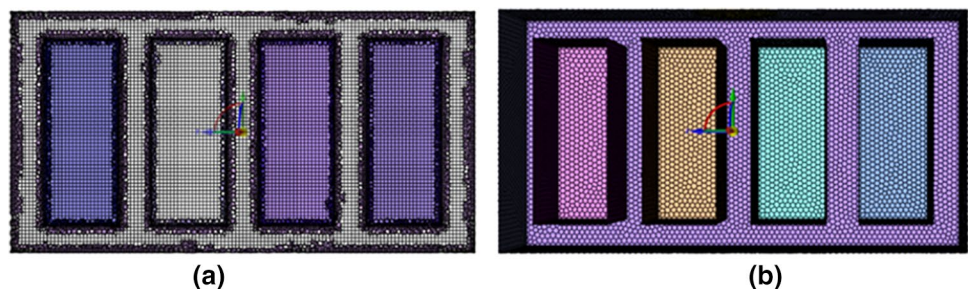


Fig. 4 Numerical results of grid dependency test

Table 2 k- $\epsilon$  equation constant

$C_1$	$C_2$	$C_u$	$\sigma_k$	$\sigma_\epsilon$	$\sigma_T$
1.44	1.92	0.09	1.0	1.3	0.9–1.0

Fig. 3 Plan view of the battery pack mesh model. a Internal grid; b surface grid



### Validation of the CFD method

To validate the accuracy of the thermal impact model for the lithium-ion single cell, a structural model validation for the lithium-ion single cell was conducted. Temperature measuring points were positioned at the front, side, and upper surface center points of the power battery. Subsequently, the transient thermal impact simulation of the lithium-ion battery monomer was executed, and a comparison between the simulation and experimental temperatures [34] at the three measuring points of the battery monomer is presented in Fig. 5. It is evident that the disparity between the simulated and experimental temperatures at the three measuring points is below 3 °C, with an error margin within 10%. Therefore, the effectiveness of the thermal impact model for the lithium-ion battery monomer is validated, rendering it suitable for subsequent battery pack heat dissipation investigations.

### Results and discussion

#### Influence of inlet and outlet diameter on heat dissipation

Based on the dimensions of the transverse wall of the battery pack, four distinct inlet and outlet diameters ( $D$ ) were devised for the investigation of battery pack heat dissipation. Specifically,  $D$  value changes from 120 to 210 mm, with an interval of 30 mm, with a single inlet and outlet for 1 C discharge rate. Figures 6 and 7 illustrate the temperature distribution within the central section of the battery pack and the relationship between  $T_{max}$  and  $\Delta T_{max}$  of the battery module concerning the dimensions of the inlet and outlet of the battery pack.

Observations indicate significant influence of different values of  $D$  on  $T_{max}$  when the inlet velocity is  $5 \text{ ms}^{-1}$  and the discharge rate is 1 C. At  $D_1$  of 120 mm, the  $T_{max}$  of the

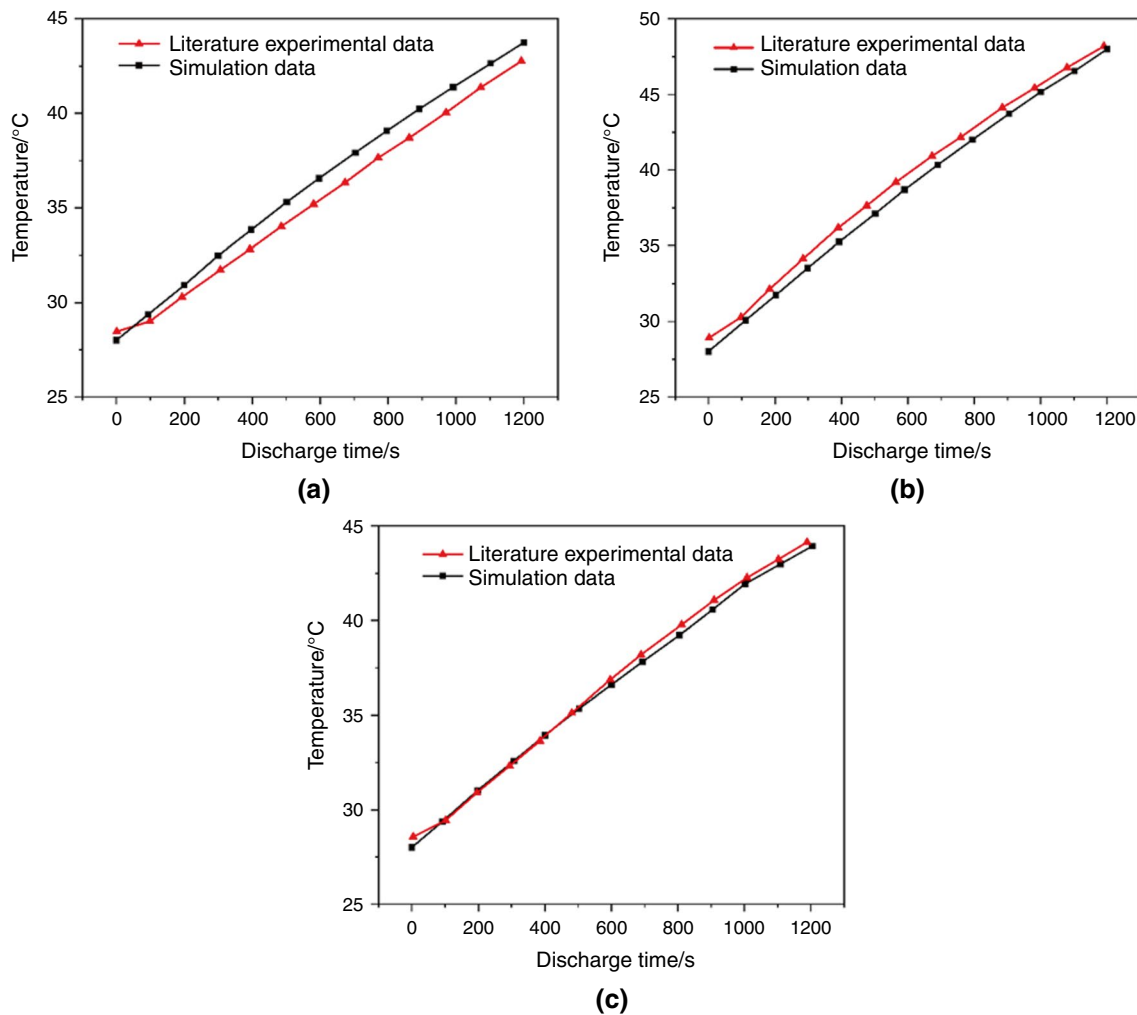
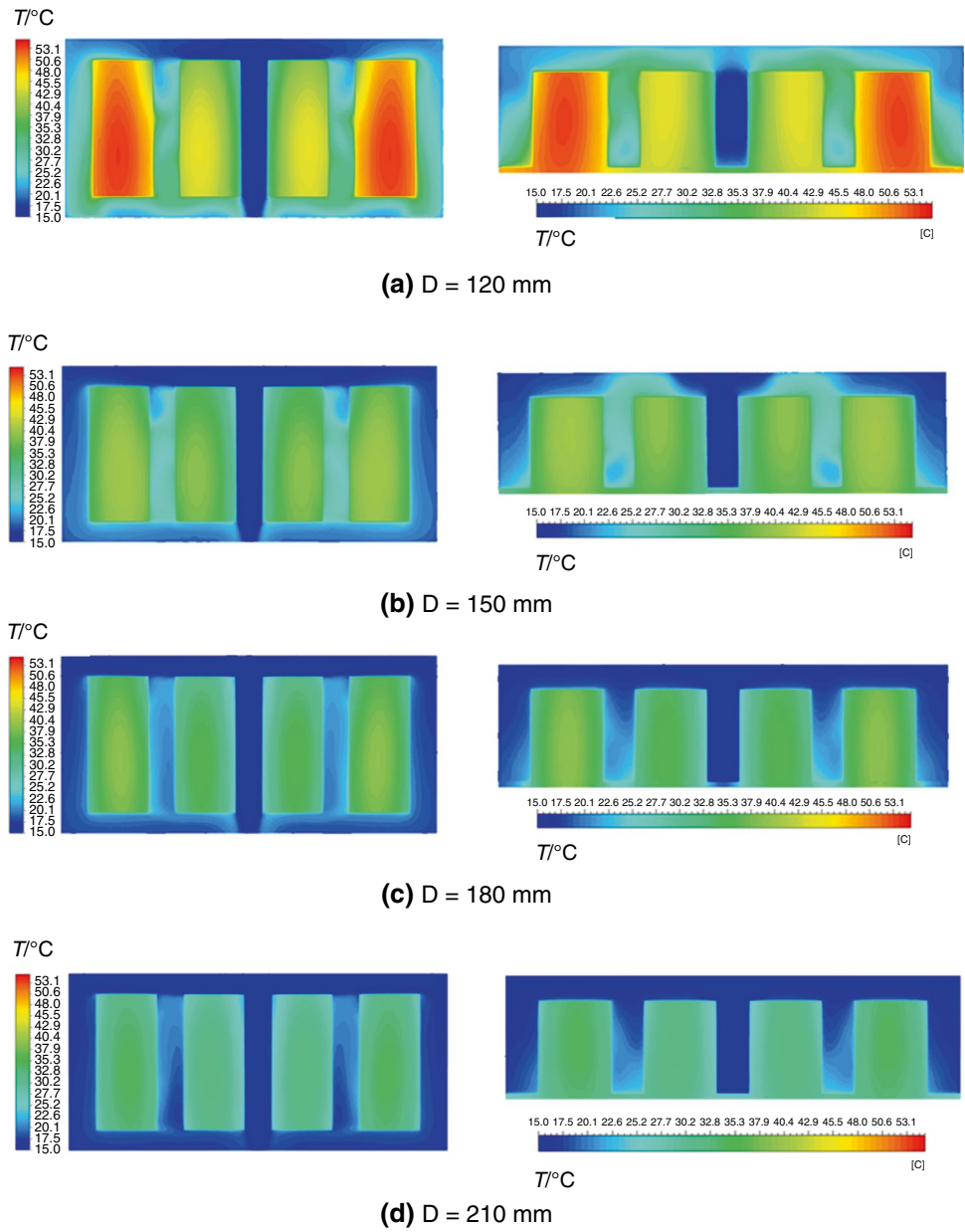


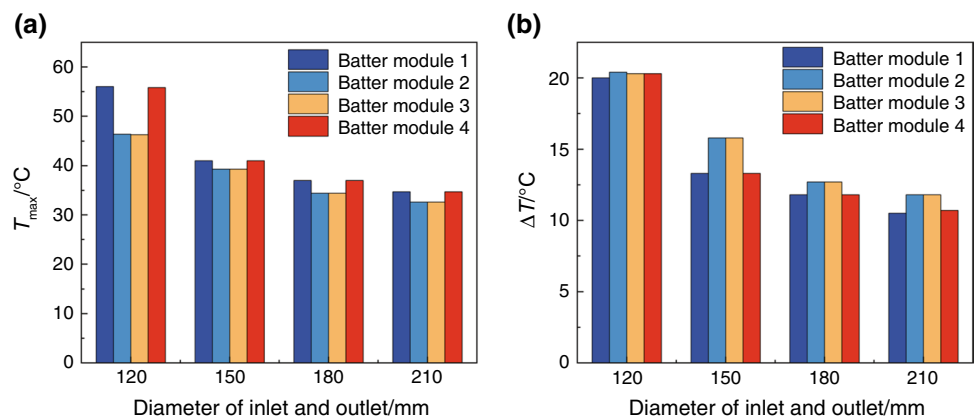
Fig. 5 Variation of battery surface center point temperature with time. a battery front; b battery side; c battery upper surface



**Fig. 6** The temperature contours under different sizes of inlet and outlet air inlets



**Fig. 7** Relationship between the temperature of the battery module and the inlet and outlet air sizes



battery pack registers 56 °C, whereas at  $D_2$  of 150 mm, it drops to 41 °C, a 15 °C decrease compared to  $D_1$ , notably improving the heat dissipation effect. Furthermore,

with  $D_3$  at 180 mm and  $D_4$  at 210 mm, the  $T_{\max}$  of the battery pack decreases to 37 °C and 34.7 °C respectively, which is 19 °C and 21.3 °C lower than that of  $D_1$ , representing reductions of 19 °C and 21.3 °C from  $D_1$ , indicating enhanced heat dissipation with larger inlet and outlet sizes. However, the influence on heat transfer gradually diminishes with diameter increase.

In addition, it is evident that battery modules 1 and 4 on both sides of the battery pack exhibit poor heat dissipation performance due to inlet and outlet location and air duct shape. At  $D_1$  situation, the  $\Delta T_{\max}$  of the battery module reaches its peak, while overall temperature uniformity of the remaining three battery packs sees significant enhancement. At the same time, enlarging the diameter of the inlet and outlet from 120 to 210 mm leads to a decrease in the  $\Delta T_{\max}$  from 20.4 to 10.7 °C, accompanied by a reduction in  $T_{\max}$ . This is attributed to enhanced airflow volume in the flow channel between battery modules, resulting in significant  $T_{\max}$  and  $\Delta T_{\max}$  reduction.

## Influence of the number of air inlet and outlet on heat dissipation

The effect of inlet and outlet numbers on the battery pack heat dissipation was investigated while maintaining a constant total area for the inlet and outlet. The layout for three inlet and outlet number configurations depicted in Figs. 8 and 9 showcases temperature contours of the battery pack with inlet and outlet diameters set at 210 mm, 149 mm, and 121 mm, respectively. Additionally, the bar chart depicting  $T_{\max}$  and  $\Delta T_{\max}$  variations of battery modules within the battery pack with different inlet and outlet numbers is presented in Fig. 10. Notably, at a discharge rate 2 C and the inlet velocity of 5 ms<sup>-1</sup>, as  $N$  changes from 1 to 3,  $T_{\max}$  is 93.8 °C, 88.6 °C, and 94.6 °C, respectively. Moreover, with  $N$  set at 2,  $T_{\max}$  is 5.2 °C lower than that of under  $N$  of 1 and 6 °C lower than that under  $N$  of 3. The overall temperature uniformity of the battery pack under  $N$  of 2 notably surpasses that under  $N$  of 1 and 3. Therefore, it demonstrates that a battery pack exhibits optimal heat dissipation performance with  $N$  set at 2, while performance is poorest with  $N$  set at 3. Furthermore, the  $T_{\max}$  of a battery pack under  $N$  of 2 is significantly lower than that under  $N$  of 1

**Fig. 8** Battery pack layout at different inlet and outlet numbers

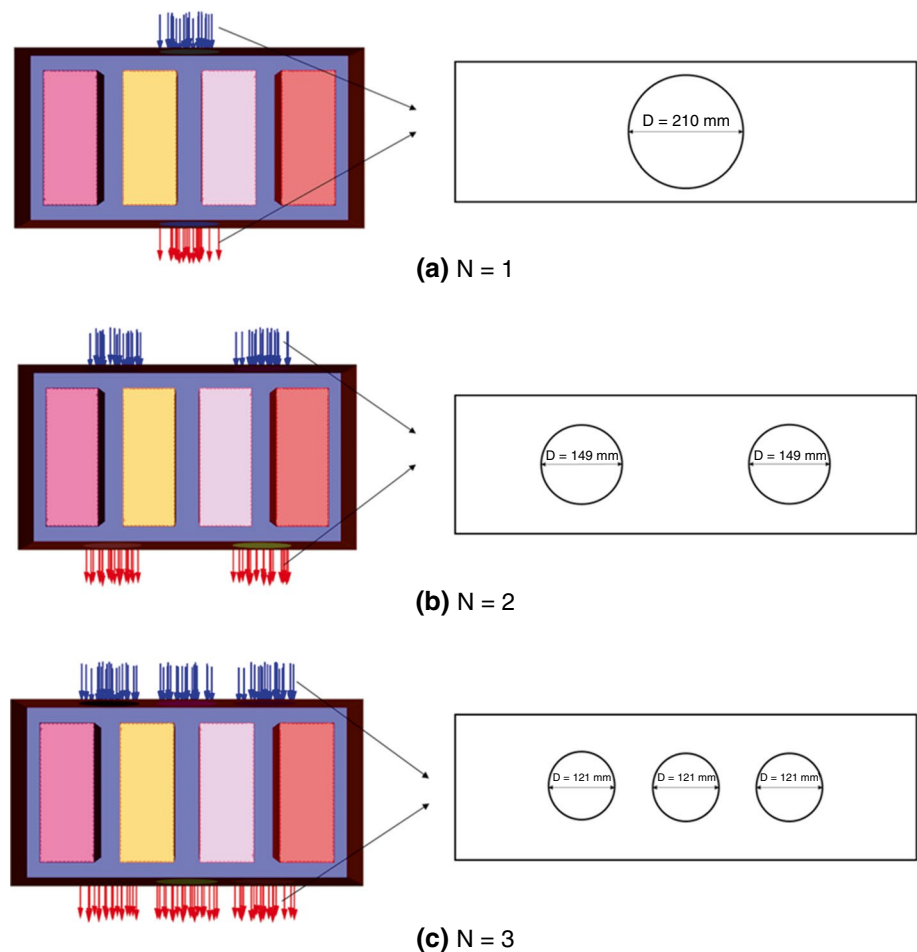


**Fig. 9** The temperature contours under different air inlet and outlet numbers

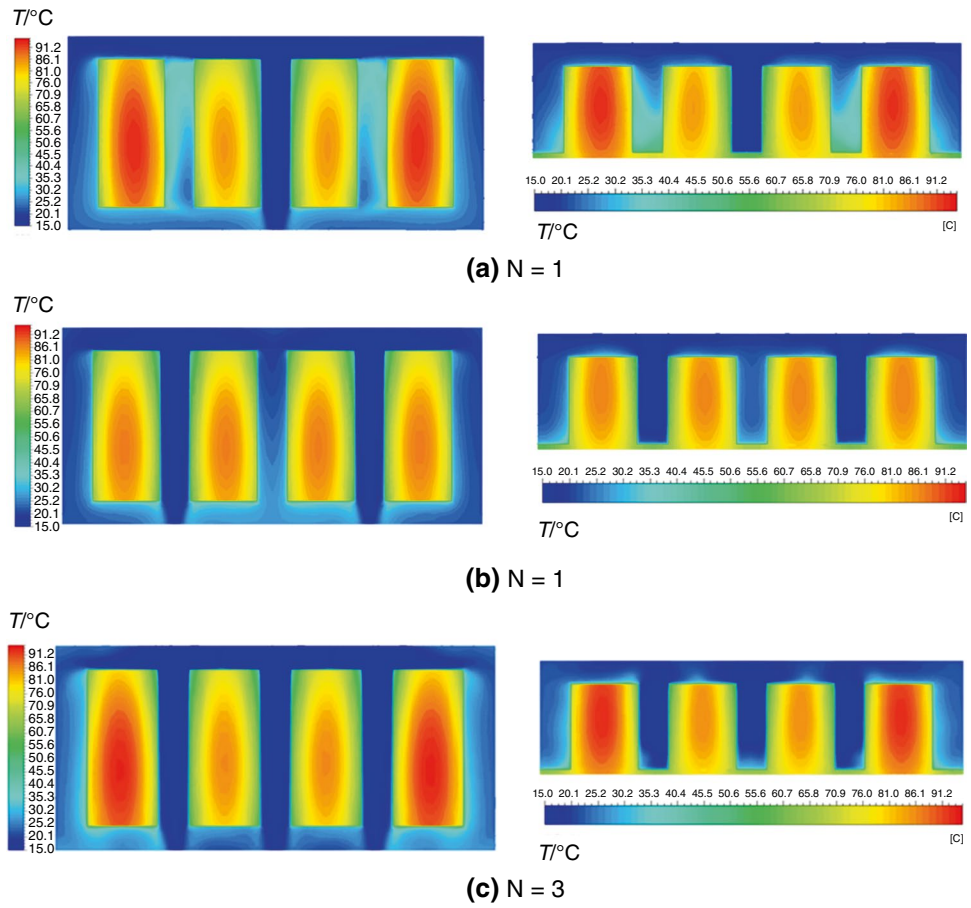
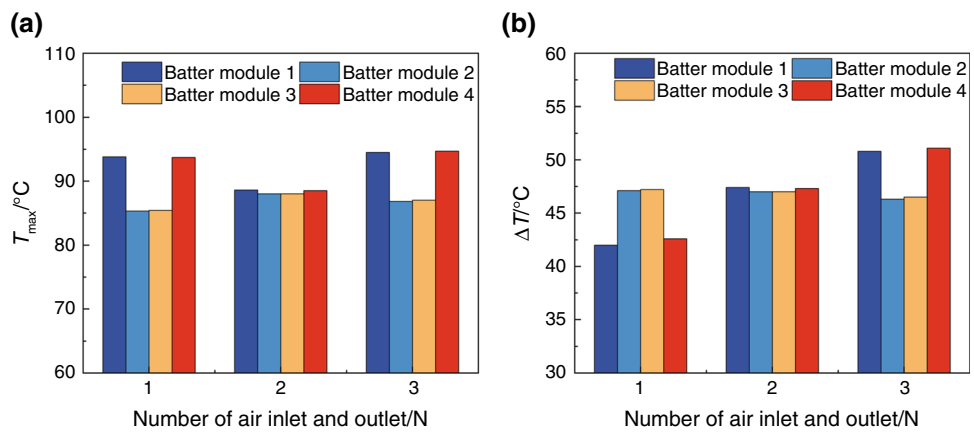


**Fig. 10** Relationship between battery module temperature and inlet and outlet air numbers



and 3, indicating superior heat dissipation performance. The  $T_{max}$  of the four battery modules in the battery pack is nearly identical under  $N$  of 2, with the overall temperature uniformity being the best. Conversely, under  $N$  of 1, the  $\Delta T_{max}$  between battery modules 2 and 3 is 47.4 °C, while under  $N$  of 2, the maximum temperature difference among the four battery modules remains consistent. Compared to

$N$  of 1, the  $\Delta T_{max}$  among the four battery modules under  $N$  of 2 is reduced by only 0.2 °C. Therefore, the temperature uniformity of the battery modules under  $N$  of 1 and 2 is similar. Conversely, the battery pack under  $N$  value of 3 exhibits the poorest temperature uniformity, with a  $\Delta T_{max}$  of 51 °C. Therefore, the comprehensive heat dissipation performance is optimal under  $N$  of 2.



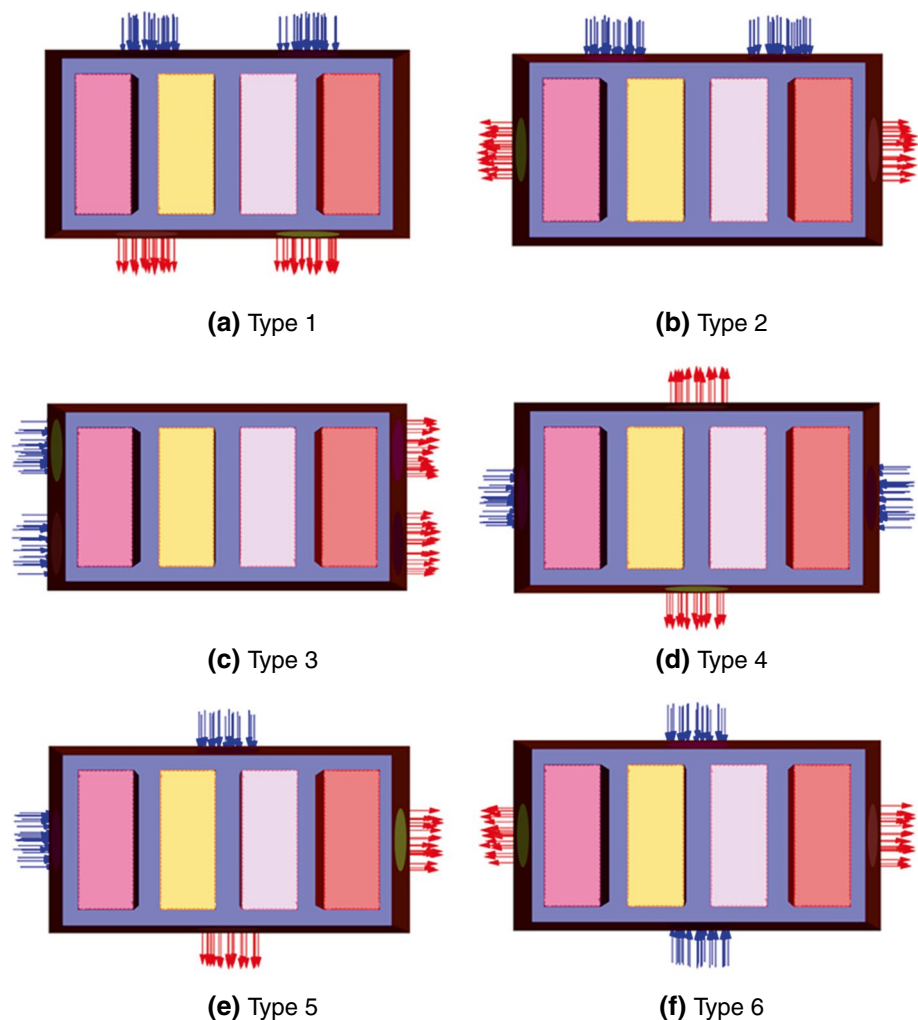
## Influence of inlet and outlet air modes on heat dissipation

Through the above analysis, the number of inlet and outlet was selected as 2, and battery packs with six inlet and outlet air modes were designed for further heat dissipation research. The specific inlet and outlet air types are shown in Fig. 11.

Aiming at the six different air inlet and outlet configurations of the battery pack, the temperature contours and velocity charts at 2 C discharge rate are depicted in Fig. 12. Battery modules are sequentially numbered from 1 to 4, left to right. The density of the trace reflects the airflow within the channel. With the first method, airflow is evenly distributed, albeit with reduced airflow above the module, resulting in satisfactory overall temperature uniformity despite limited heat dissipation efficiency and negligible  $\Delta T_{\max}$ . Type 2 demonstrates superior heat dissipation compared to type 1 due to increased airflow, particularly on

the sides, resulting in poorer heat dissipation for modules 2 and 3. Conversely, type 4 resembles type 1, with limited airflow between modules, favoring better side heat dissipation over the middle module. Type 5 experiences airflow blockage, notably lowering heat dissipation efficiency at module 4, worsening overall uniformity. Lastly, airflow velocity of type 6 diminishes between modules, intensifying turbulence in the middle, reducing heat dissipation for modules 1 and 4. Figure 13 illustrates maximum temperature and temperature differences among the six layouts, with maximum temperatures ranging from 88.6 to 93.6 °C. Type 2 exhibits the lowest maximum temperature, reflecting superior heat dissipation. The maximum temperatures of the modules vary, with type 1 displaying the smallest disparities and best overall uniformity. Moreover, maximum temperature differences range from 42.6 to 50 °C, with type 5 demonstrating the best uniformity and type 3 the worst. Overall, type 2 boasts the most effective cooling performance, considering maximum temperature and uniformity.

**Fig. 11** Six different inlet–outlet types of BTMSs



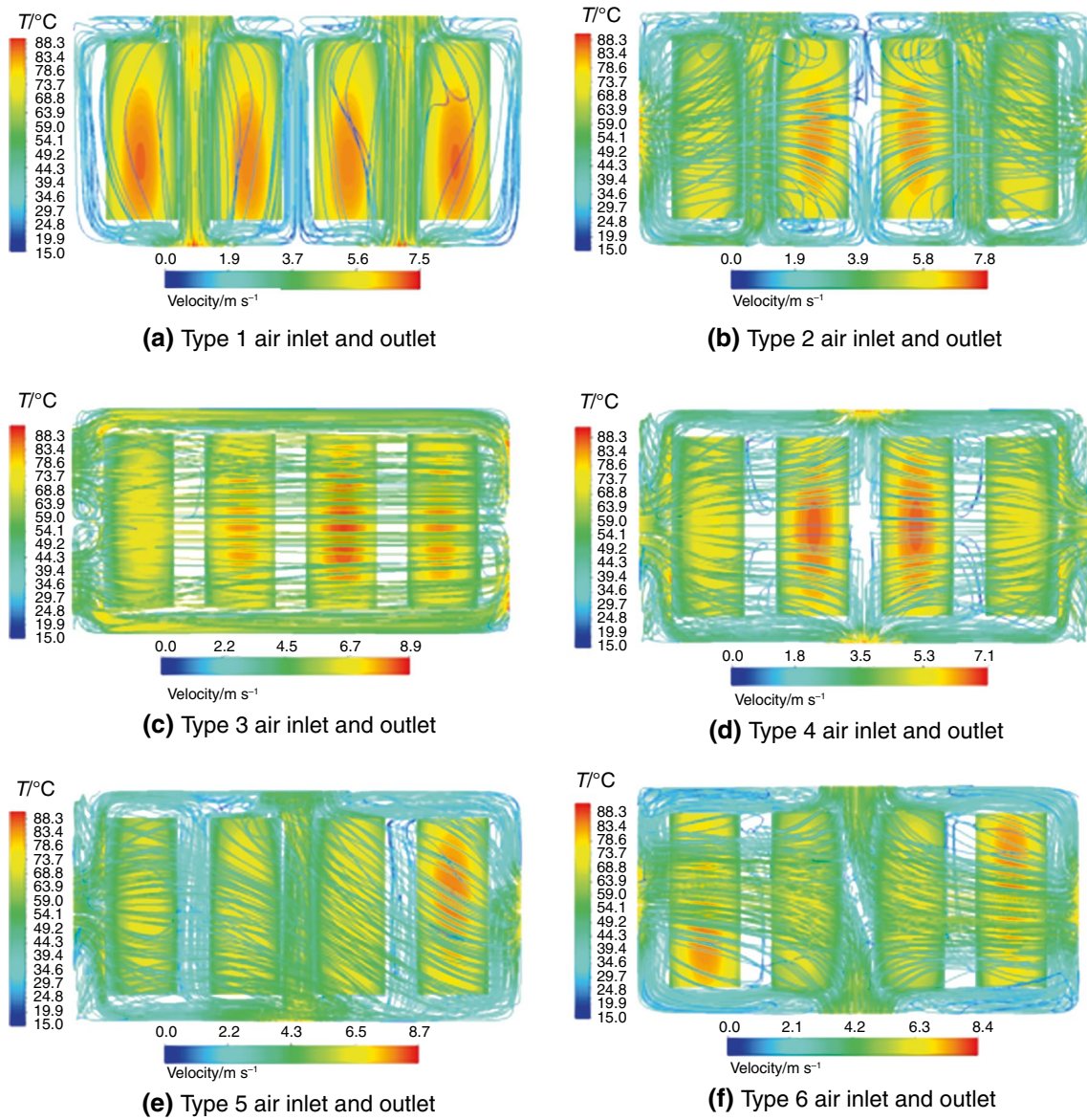
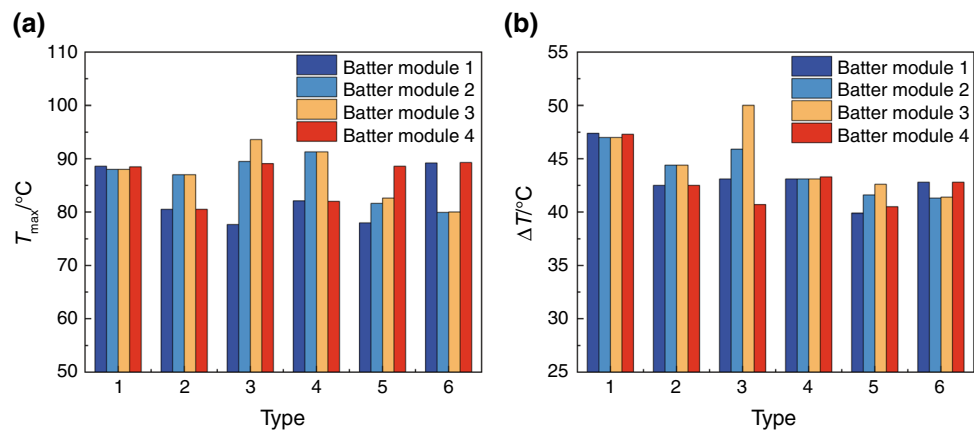


Fig. 12 The temperature contours and velocity trace under six types of BTMSs

Fig. 13 Relationship between battery module temperature and inlet–outlet types



## The effect of forced convection wind speed on heat dissipation

Based on the previous research, the battery pack heat dissipation model of type 2 with the best comprehensive heat dissipation effect was selected as the research model of forced air-cooled. The battery pack heat dissipation under different inlet velocities ( $V_{in}$ ) was investigated. Inlet velocities range from 5 to 30  $\text{ms}^{-1}$ , incrementing in 5  $\text{ms}^{-1}$  intervals. Figure 14 depicts the corresponding changes in  $T_{max}$  and  $\Delta T_{max}$  within the battery pack with altering inlet velocities.

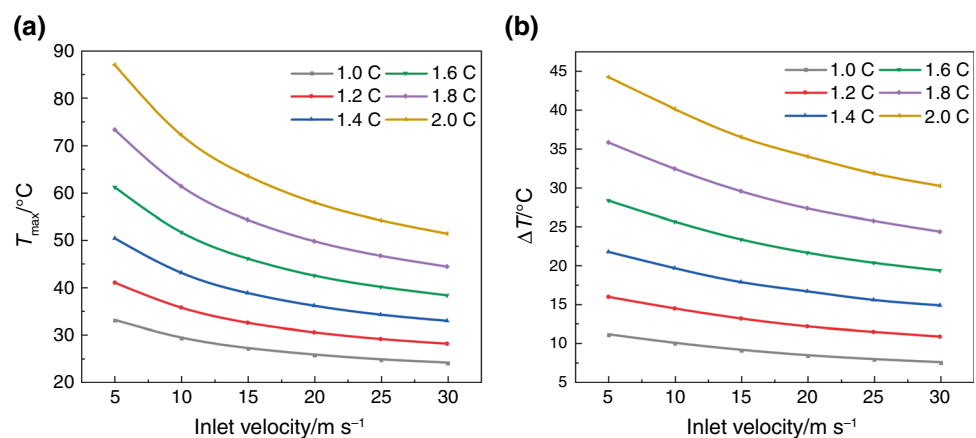
It is demonstrated that as  $V_{in}$  increases from 5 to 10  $\text{ms}^{-1}$ ,  $T_{max}$  of the battery pack decreases by 14.8  $^{\circ}\text{C}$ , and  $\Delta T_{max}$  decreases by 4.1  $^{\circ}\text{C}$ . Conversely, when  $V_{in}$  further increases from 25 to 30  $\text{ms}^{-1}$ , the  $T_{max}$  experiences only a 3.8  $^{\circ}\text{C}$  decrease, with  $\Delta T_{max}$  decreasing merely by 1.8  $^{\circ}\text{C}$ . The trend indicates that a gradual decrease in  $T_{max}$  and  $\Delta T_{max}$  as inlet velocity rises, but the enhancement of battery pack heat dissipation is gradually weakened. The suggested temperature range for such lithium-ion batteries typically extends from 25 to 45  $^{\circ}\text{C}$  [35]. Nevertheless, due to the limited power of the fan, the inlet velocity of forced air-cooled cannot be endlessly increased. Consequently, forced air-cooling suffices to meet the battery pack heat dissipation requirements at temperatures below a 1.6 C discharge rate. Beyond this threshold, alternative heat dissipation methods become necessary to maintain the battery pack within the optimal temperature range. When the discharge rate is greater than 1.6 C, additional heat dissipation methods are required to maintain the battery pack within the optimal temperature range.

## Conclusions

In this paper, the lithium-iron phosphate power battery pack of a military hybrid armored vehicle was selected to study its heat dissipation characteristics at an altitude of 4000 m on the plateau. The main conclusions are as follows:

- (1) The effect of structure parameters of battery pack was investigated on its air-cooled heat dissipation performance. The results indicate that when there is only one inlet and outlet, size increasing enhances the heat dissipation performance. As the inlet and outlet diameters increase from 120 to 210 mm, the maximum temperature difference of the battery module decreases from 20.4 to 10.7  $^{\circ}\text{C}$ . This is predominantly due to the increased convective heat transfer coefficient resulting from the larger volume of inlet air.
- (2) Keeping the inlet and outlet air volumes as constant, the battery pack achieves optimal heat dissipation performance when there are two inlets and outlets. The second inlet and outlet configuration, with the air inlet located at the front of the battery pack and the outlet on its side, exhibits the most comprehensive heat dissipation effect. Specifically, the maximum temperature of the battery pack is 5.2  $^{\circ}\text{C}$  when there are two inlets and outlets, which is lower than that of one or three inlets and outlets.
- (3) Building upon the second type of inlet and outlet configuration, the effect of inlet velocity for forced air-cooled was investigated, ranging from 5 to 30  $\text{ms}^{-1}$ . The results demonstrate that higher inlet velocity correlates with lower maximum temperatures of the battery pack. However, the rate of temperature decrease gradually slows down as the inlet velocity increases. Additionally, forced air-cooled heat dissipation can only maintain the temperature of battery packs within an optimum range for discharge rates of up to 1.6 C.

**Fig. 14** Temperature variation of battery pack at different inlet velocities



**Acknowledgements** The authors gratefully acknowledge financial support from Key Laboratory of Electromechanical Equipment Security in Western Complex Environment for State Market Regulation (CQTI-XBJD-KFKT202204) and State Administration for Market Regulation (2022MK108).

**Authors contributions** Project PI was done by Yunfei Yan and Ziqiang He; Yunfei Yan was involved in methodology; Yonghong Wu and Rongtian Wang helped in software; Yonghong Wu contributed to manuscript writing; Rongtian Wang, Jingxiang YOU, and Zongguo Xue helped in validation; Data curation was done by Jinhua Wu; Yonghong Wu and Rongtian Wang were involved in formal analysis.

## References

- Murshed SMS, De Castro CAN. A critical review of traditional and emerging techniques and fluids for electronics cooling. *Renew Sustain Energy Rev.* 2017;78:821–33.
- You J, Xue Z, He Z, et al. Hydrogel use in burn therapy, thermal management, wastewater treatment and fire fighting: a review. *Environ Chem Lett.* 2023;21(6):3273–328.
- Yan Y, Zhang C, Liu Y, et al. Numerical study on hotspots adaptive cooling and thermal-hydraulic performance enhancement of fractal microchannel heat sink embedded with hydrogels. *Int J Therm Sci.* 2022;172: 107272.
- Cui Z, Yang X, Yue J, et al. A review of digital twin technology for electromechanical products: evolution focus throughout key lifecycle phases. *J Manuf Syst.* 2023;70:264–87.
- Chen L, Liu H, Qi H, et al. High-electromechanical performance for high-power piezoelectric applications: fundamental, progress, and perspective. *Prog Mater Sci.* 2022;127: 100944.
- Guo L, Han ST, Zhou Y. Electromechanical coupling effects for data storage and synaptic devices. *Nano Energy.* 2020;77: 105156.
- Magisetty RP, Cheekuramelli NS. Additive manufacturing technology empowered complex electromechanical energy conversion devices and transformers. *Appl Mater Today.* 2019;14:35–50.
- Jiaqiang E, Ding J, Chen J, et al. Process in micro-combustion and energy conversion of micro power system: a review. *Energy Convers Manage.* 2021;246: 114664.
- Barzegar-Kalashani M, Seyedmahmoudian M, Mekhilef S, et al. Small-scale wind turbine control in high-speed wind conditions: a review. *Sustain Energy Technol Assess.* 2023;60: 103577.
- Xue Z, Yan Y, Shen K, et al. Thermal-hydraulic performance analysis of a liquid-jet-cooled heat sink with a macroscopic porous flow diverter. *Appl Therm Eng.* 2023;230: 120654.
- He Z, Yan Y, Zhang L. Thermal-hydraulic investigation on micro heat sinks with ribbed pin-fin arrays and single heating input: parametrical study[J]. *J Therm Anal Calorim.* 2022: 1–17.
- Yan Y, Xue Z, Xu F, et al. Numerical investigation on thermal-hydraulic characteristics of the micro heat sink with gradient distribution pin fin arrays and narrow slots. *Appl Therm Eng.* 2022;202: 117836.
- Smith KC, Chiang YM, Carter WC. Maximizing energetic efficiency in flow batteries utilizing non-Newtonian fluids. *Electrochem Soc.* 2014;161(4):A486.
- Gnadt AR, Speth RL, Sabnis JS, et al. Technical and environmental assessment of all-electric 180-passenger commercial aircraft. *Prog Aerosp Sci.* 2019;105:1–30.
- Steinberg DS. *Cooling techniques for electronic equipment.* New York, 1980.
- Belady CL. Design considerations for air cooling electronic systems in high altitude conditions. *IEEE Trans Compon Packag Manuf Technol Part A:* 1996;19(4):495–500.
- Hall DA. Prediction of electronic component temperatures at high altitude using low altitude measurements. In: *Fifth Annual IEEE Semiconductor Thermal and Temperature Measurement Symposium.* IEEE, 1989: 121–125.
- Xu G. Thermal performance prediction for high power processors at high altitude. *ASME Int Mech Eng Congr Expos.* 2005;42177:549–54.
- Wong H, Peck RE. Experimental evaluation of air-cooling electronics at high altitudes. *J Electron Packag.* 2001;123(4):356–65.
- Elsayed ML, Mesalhy O, Kizito JP, et al. Performance of a guided plate heat sink at high altitude. *Int J Heat Mass Transf.* 2020;147: 118926.
- Renau J, Barroso J, Lozano A, et al. Design and manufacture of a high-temperature PEMFC and its cooling system to power a lightweight UAV for a high altitude mission. *Int J Hydrogen Energy.* 2016;41(43):19702–12.
- Lu Z, Yu X, Wei L, et al. Parametric study of forced air cooling strategy for lithium-ion battery pack with staggered arrangement. *Appl Therm Eng.* 2018;136:28–40.
- Shengxin E, Liu Y, Cui Y, et al. Effects of composite cooling strategy including phase change material and cooling air on the heat dissipation performance improvement of lithium ion power batteries pack in hot climate and its catastrophe evaluation. *Energy.* 2023;283: 129074.
- Shengxin E, Cui Y, Liu Y, et al. Effects of the different phase change materials on heat dissipation performances of the ternary polymer Li-ion battery pack in hot climate. *Energy.* 2023;282: 128805.
- Xu S, Wan T, Zha F, et al. Numerical simulation and optimal design of air cooling heat dissipation of lithium-ion battery energy storage cabin. *J Phys: Conf Ser IOP Publ.* 2022;2166(1): 012023.
- Xie J, Ge Z, Zang M, et al. Structural optimization of lithium-ion battery pack with forced air cooling system. *Appl Therm Eng.* 2017;126:583–93.
- Hasan HA, Togun H, Abed AM, et al. A novel air-cooled Li-ion battery (LIB) array thermal management system: a numerical analysis[J]. *Int J Therm Sci.* 2023;190: 108327.
- Li W, Xiao M, Peng X, et al. A surrogate thermal modeling and parametric optimization of battery pack with air cooling for EVs. *Appl Therm Eng.* 2019;147:90–100.
- Zhang C, Yan Y, Shen K, Xue Z, You J, He Z. Comparative analysis of combustion stability and flow performance in micro combustor based on the synergistic action of slotted blunt body and front-baffle. *Appl Ther Eng.* 2024;237: 121802.
- Shahid S, Agelin-Chaab M. Development and analysis of a technique to improve air-cooling and temperature uniformity in a battery pack for cylindrical batteries. *Therm Sci Eng Progr.* 2018;5:351–63.
- Zhang C, Yan Y, Shen K, Xue Z, You J, Yonghong Wu, He Z. Study on synergistic heat transfer enhancement and adaptive control behavior of baffle under sudden change of inlet velocity in a micro combustor. *J Clean Prod.* 2023;434: 139856.
- Feng S, Shan S, Lai C, Chen J, Li X, Mori S. Multi-objective optimization on thermal performance and energy efficiency for battery module using gradient distributed Tesla cold plate. *Energy Convers Manage.* 2024;308: 118383.
- Zhang F, Lin A, Wang P, et al. Optimization design of a parallel air-cooled battery thermal management system with spoilers. *Appl Therm Eng.* 2021;182: 116062.

34. Wu F, Rao Z. The lattice Boltzmann investigation of natural convection for nanofluid based battery thermal management. *Appl Therm Eng.* 2017;115:659–69.
35. Patil A, Choi J W. Review of issue and challenges facing rechargeable nanostructured lithium batteries. In: 2006 IEEE nanotechnology materials and devices conference. IEEE, 2006, 1: 196-197.

Springer Nature or its licensor (e.g. a society or other partner) holds exclusive rights to this article under a publishing agreement with the author(s) or other rightsholder(s); author self-archiving of the accepted manuscript version of this article is solely governed by the terms of such publishing agreement and applicable law.

**Publisher's Note** Springer Nature remains neutral with regard to jurisdictional claims in published maps and institutional affiliations.